Power Electronic Systems
Laboratory

Proceedings of the International Power Electronics Conference (ECCE Asia 2018), Niigata, Japan, May 20-24, 2018

Exploration of the Design and Performance Space of a High Frequency 166 kW / 10 kV SiC Solid-State Air-Core Transformer

P. Czyz,
T. Guillod,
F. Krismer,
J. W. Kolar

Eidgenössische Technische Hochschule Zürich
Swiss Federal Institute of Technology Zurich

Exploration of the Design and Performance Space of a High Frequency 166 kW / 10 kV SiC Solid-State Air-Core Transformer

Piotr Czyz, Thomas Guillod, Florian Krismer and Johann W. Kolar
Power Electronic Systems Laboratory (PES), ETH Zurich
8092 Zurich, Switzerland
czyz@lem.ee.ethz.ch

***Abstract*— With the availability of 10 kV SiC MOSFETs with low Zero Voltage Switching (ZVS) losses, Medium-Voltage (MV) converters, e.g., Solid-State Transformers (SST), capable of operation at very high switching frequencies become feasible. However, the optimization of MV and Medium-Frequency (MF) transformer of the dc–dc converter stage of a high power SST reveals that only limited improvements in efficiency and weight result for switching frequencies exceeding 50 kHz. Therefore, air-core transformers are expected to enable a realization with lower weight and, at the same time, simplified insulation coordination. This paper presents a comprehensive exploration of the design and performance spaces (efficiency, mass, volume) of a conventional, i.e., a magnetic-core based, and an air-core transformer employed in a resonant dc–dc converter with input and output voltages of 7 kV and a rated power of 166 kW. As a result, comparable efficiencies are achievable for both transformers (99.3% and 99.0%), but the SST with air-core transformer at a switching frequency of 103.6 kHz features 41% of the mass (10.3 kg) of a conventional transformer (24.9 kg at a switching frequency of 48.5 kHz). Accordingly, air-core transformers are of special interest for future weight-critical SST applications, e.g., in More Electric Aircraft and More Electric Ships.**

***Keywords*—Air-Core Transformer, Power Electronics, Medium-Frequency, Medium-Voltage, Solid-State Transformers, Inductive Power Transfer.**

I. Introduction

Medium-Voltage and Medium-Frequency (MV/MF) transformers represent core elements of Solid-State Transformers (SSTs) and enable galvanic isolation and high step-down or step-up voltage ratios at high conversion efficiencies, high power densities, and low mass. Thus, SSTs are of special interest in aerospace applications [1] (particularly in the field of commercial transport aircraft), in maritime applications [2] and, due to advanced control capabilities, also in general smart grid applications [3]. The trend for More Electric Aircraft (MEA) already exists in the industry for years, resulting in aircraft with hydraulic and pneumatic systems, partially exchanged by electric systems (e.g., in Airbus A380 or in Boeing 787). More recently, thanks to emerging advanced technologies in composites, electric batteries, and motors, further new design concepts regarding the propulsion architecture are developed, i.e., Electrical Propulsion (EP) architectures. EP cover all-electric, hybrid and Turboelectric Distributed Propulsion systems (TeDP). An all-electric aircraft still, due to the limitation of batteries, is feasible only for small, short-haul aircraft. Therefore, in the area of long-haul commercial aircraft only hybrid and TeDP architectures are considered. In hybrid propulsion systems one or more of the gas turbines of a conventional aircraft is replaced by an electric motor with fan, as e.g., in the hybrid-electric flight demonstrator *E-Fan X* [4]. However, the vast majority of the thrust is still generated by gas turbines. TeDP architectures, apart from the gas turbo-generators, utilize an array of motor driven fans, as shown in **Fig. 1**. In this architecture the primary function of the turbogenerators is to generate the electric power which is then transferred to distributed electric fans, where the thrust is generated. The power rating of the motors driving the fans might reach up to $4\,\mathrm{MW}$ [5], therefore, initial studies imply using superconducting electric components. However, due to challenges with lightweight, efficient, and reliable cryocoolers, recent studies also focus on conventional ambient temperature systems [5]. To reduce the losses and masses of the components used in conventional electric systems, a HVDC electric bus is considered. Depending on which parameter is minimized (electrical system's mass or losses) the recommended optimum HVDC bus operating voltage is ranging from $\pm 3\,\mathrm{kV}$ to $\pm 4.5\,\mathrm{kV}$ [6]. A basic concept of a TeDP aircraft electric power system architecture with the $\pm 3.5\,\mathrm{kV}$ bus voltage is presented in **Fig. 2**. In the context of safety and redundancy considerations, such a system is expected to incorporate a circuit breaker between the two dc buses to facilitate continued operation with the working system in case of a severe failure. Advanced state-of-the-art solutions are hybrid dc circuit breakers [7] that incorporate a parallel connection of a mechanical circuit breaker and a string of IGBTs. Pure solid-state dc circuit breakers (SSCB) featuring low losses which could be realized with MV SiC MOSFETs, are, however, still subject to research [8]. Due to the limited flexibility of circuit breakers, also a light-weight air-core SST could be used instead, which provides increased reliability by reason of galvanic isolation, is tolerant with regard to different dc bus voltages, and features overcurrent limitation. In addition to this, further applications of SSTs are highly likely to appear in future TeDP aircraft, e.g., to realize power conditioning units for battery energy storages.

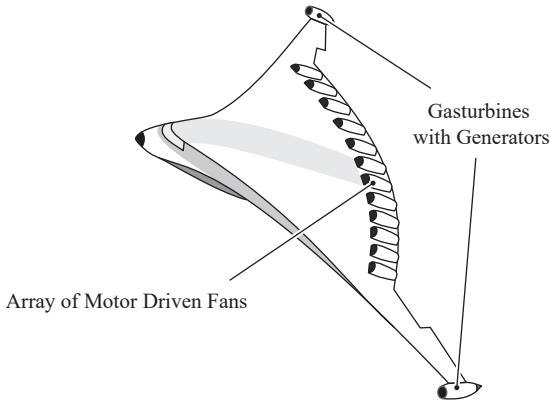

Fig. 1. Concept of TeDP aircraft, based on [5]. Two turbogenerators, i.e., turbine engines driving electrical generators, are located on the wingtips. The electric power from the turbogenerators is distributed to an array of motor driven fans located on the trailing edge of the aircraft body.

State-of-the-art high efficiency power converters typically feature gravimetric power densities up to $5\,\mathrm{kW/kg}$ (cf. **Fig. 3**) [9]. TeDP aircraft applications, however, rather require values greater than $\gamma = 10\,\mathrm{kW/kg}$, e.g., $\gamma = 14\,\mathrm{kW/kg}$ at an efficiency of $\eta = 99\%$ for the combination of a dc

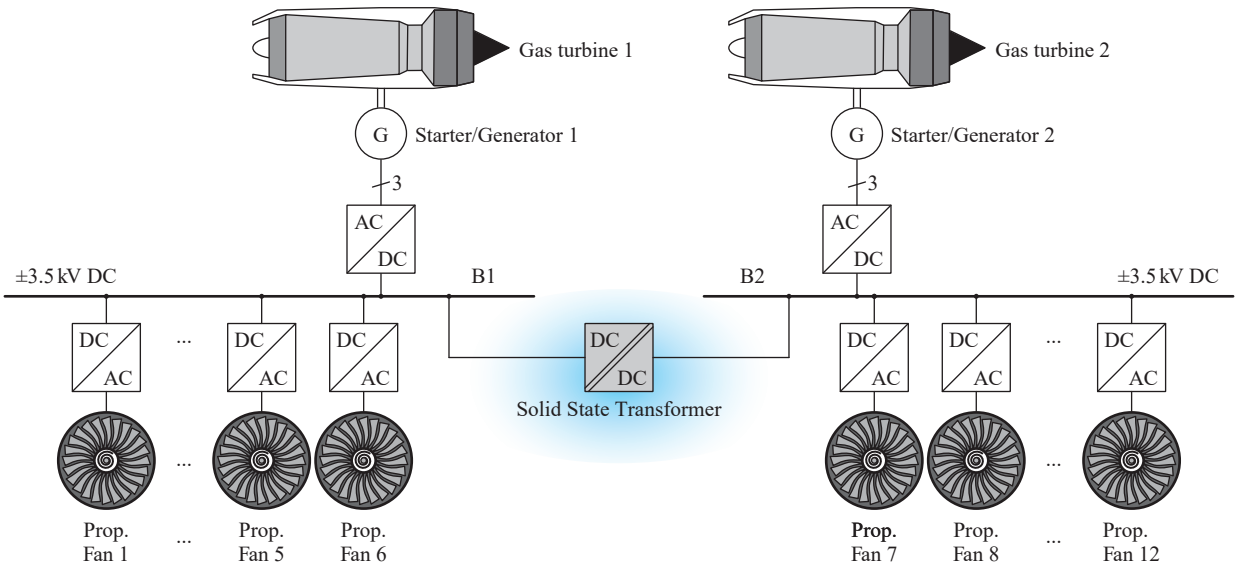

Fig. 2. Draft concept of the electric power system architecture of a TeDP aircraft. In such application the SST could be used as a power electronic link between the two HVDC buses and also fulfill the function of a dc SSCB. A SST, which is formed by parallel connection of SST cells with 166 kW of power, provides increased reliability by reason of galvanic isolation, is tolerant with regard to different dc bus voltages, and features overcurrent limitation.

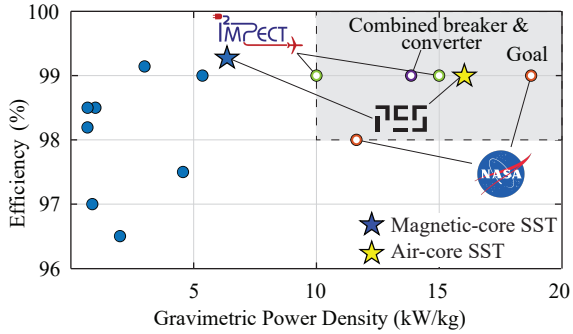

Fig. 3. The gravimetric power density and efficiency of power electronic converters for MEA applications. State-of-the-art high efficiency power converters (blue markers) are presented together with goals set by Integrated, Intelligent Modular Power Electronic Converter (I2MPECT) project [9] and The National Aeronautics and Space Administration (NASA). Proposed SST utilizes the functionality of combined circuit breaker and power converter (purple marker) [10]. The air-core and magnetic core SST designs presented in this paper are shown with stars.

circuit breaker and a power converter [10]. The air-core SST design presented in this paper, cf. **Fig. 3**, could meet the high requirements of minimum gravimetric power density and system efficiency, e.g., in turboelectric aircraft.

In order to take advantage of the favorable properties of MV/MF transformers and to implement SST-specific beneficial control features, SSTs require MV power converters for generation of MF voltages suitable for the MF/MV transformer, and output voltage regulation [11]. An isolated dc–dc converter which allows for high efficiency and high power density, provides the isolation tasks of the SST. In this regard, recent literature documents that high efficiencies are achievable with Dual Active Bridge (DAB) converters and Series Resonant Converters (SRC), due to their Zero Voltage Switching (ZVS) and/or Zero Current Switching (ZCS) properties [12]–[14]. The SRC, in addition, features reduced currents at the switching instants, effectively reduces high frequency harmonic components in the currents of the MV transformer and is therefore particularly interesting for the selected application.

With the availability of MV SiC MOSFETs, very low switching losses can be achieved for ZVS operation [15], [16], which, in principle, enables MV converters to be operated with very high switching frequencies exceeding 100 kHz. In conventional MV/MF transformers, however, a substantial part of the core window is required for insulation (between the coils and between coils and core) [17]. Due to the associated low filling factor of the core window and core material limits, limited benefits are expected at high switching frequencies [18]. In contrast, the challenging insulation coordination is reduced in air-core transformers (cf. **Fig. 4**), however, lower coupling factors result. Though, recent literature reveals that high efficiency operation can still be achieved for systems with loosely coupled coils [19], [20].

This paper, therefore, explores the design and performance spaces concerning the efficiency, power density, and power to mass ratio achievable with dc–dc SRCs (cf. **Fig. 5**) employing MV and MF to High Frequency (HF) transformers with air-cores and magnetic-cores. **Table I** summarizes the specifications of the considered SRC, which is part of a multi-cell SST. **Section II** describes the model and the optimization procedure applied to the SRC with MV/MF air-core transformer and **Section III** summarizes the approach considered for the SRC with conventional MV/MF transformer. Subsequently, **Section IV** evaluates the obtained optimization results. The converter with air-core transformer is found to achieve a maximum gravimetric power density of $\gamma = 16.1\,\mathrm{kW/kg}$ at a switching frequency of $f_\mathrm{s} = 103.6\,\mathrm{kHz}$, whereas the optimal

TABLE I. Specifications of the prototype system

Electric specifications		
P	166 kW	output power
$V_{1,\mathrm{dc}}$	7 kV(±3.5 kV)	input side dc-link voltage
$V_{2,\mathrm{dc}}$	7 kV(±3.5 kV)	output side dc-link voltage
V_iso	10 kV	isolation voltage between coils of prim. and sec. sides
Litz wire		
d_litz	71 µm	single strand diameter
k_litz	28%	total fill factor of the windings (incl. the litz wire fill factor)
Thermal specifications		
$p_\mathrm{v,max}$	0.25 W/cm^2	surface related power loss density
Fixed dimensions		
w_iso	4 mm	isolation distance magnetic-core
w_iso	16 mm	isolation distance air-core

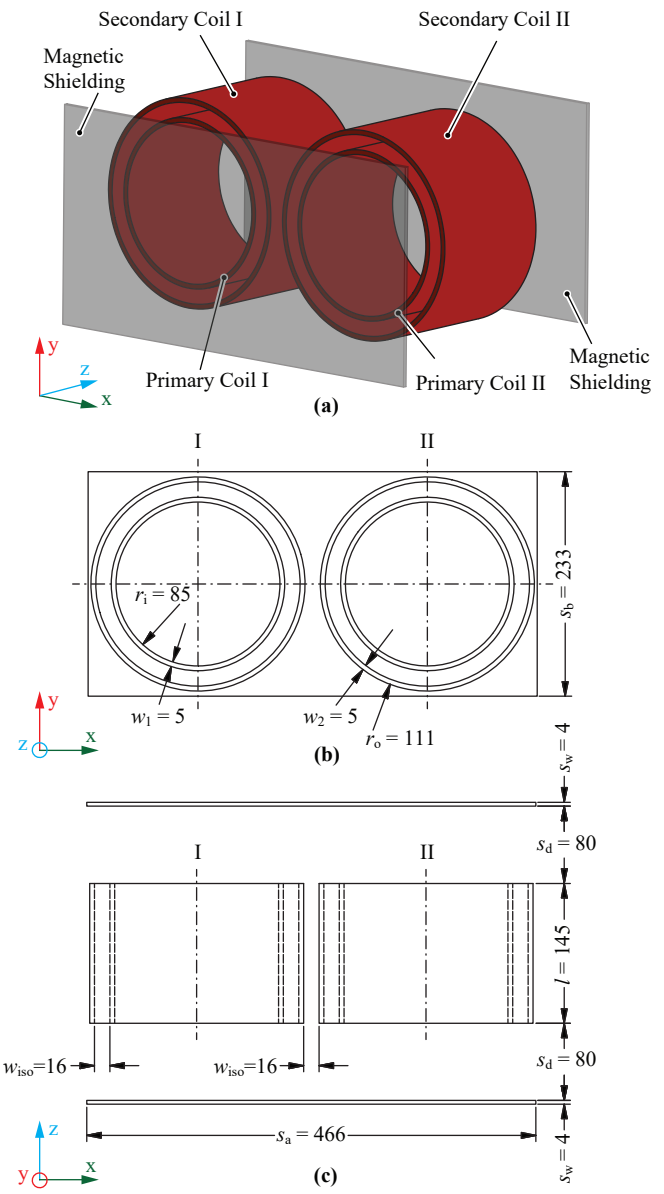

Fig. 4. (a) Schematic representation of the MV/HF air-core transformer with primary and secondary coils divided into two equal parts to provide guidance of the magnetic flux along the whole geometric path, i.e. similar to a toroidal arrangement in order to minimize the external magnetic field. Magnetic shielding plates provide the functions of back irons for stray fields at the ends of the transformer. (b) Projection from front. (c) Projection from top. Projections are in scale and all dimensions are given in mm.

solution with magnetic-core transformer is approximately one half of this gravimetric power density at a switching frequency of $f_s = 48.5\,\mathrm{kHz}$. The presented η-γ-Pareto-optimal [21] results show that a further increase of the gravimetric density of a transformer with magnetic-core is limited ($\gamma = 8.0\,\mathrm{kW/kg}$ at $\eta = 99.1\%$), whereas the design with air-core transformer can achieve comparable efficiency ($\eta = 99.0\%$) with gravimetric densities higher than $\gamma = 16.1\,\mathrm{kW/kg}$.

II. Air-core MV/MF Transformer

A. Design of the SRC

The converter design involves the calculation of the transformer's self inductances, L_1 and L_2, its mutual inductance, M, and the resonant capacitances. The inductances are obtained from the transformer geometry and the resonance capacitances are calculated in order to obtain high efficiency

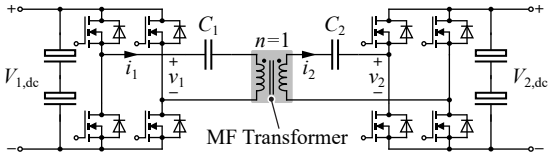

Fig. 5. Schematic drawing of the considered SRC.

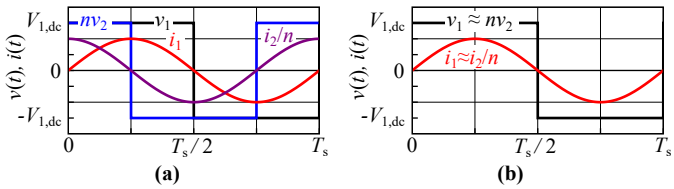

Fig. 6. AC current and voltage waveforms characterizing the operation of the dc-dc converter's MF transformer of the SRC topology: (a) waveforms resulting with the compensation technique applied to transformers with low coupling factor, $k < 0.7$; (b) waveforms resulting for the technique employed for transformers with high coupling factor, $k > 0.7$.

converter operation. Depending on the coupling factor of the investigated air-core transformer,

$$k = \frac{M}{\sqrt{L_1 L_2}}, \tag{1}$$

different compensation techniques are suitable. For low coupling factors, as e.g., in inductive power transfer [22], the SRC achieves highest efficiency if C_1 and C_2 compensate the impedances of the self inductances L_1 and L_2, respectively [22],

$$C_1 = \frac{1}{\omega_s^2 L_1}, \qquad C_2 = \frac{1}{\omega_s^2 L_2}, \tag{2}$$

and for operation with a phase shift of v_1 and v_2 of 90° (cf. **Fig. 6(a)**). In this study it is found that all feasible designs achieve relatively high coupling factors, $k > 0.7$, and as no tolerance to misalignment of coils has to be considered [22], it is therefore, more reasonable to apply the commonly used series-resonant compensation technique, i.e., to set the resonance frequency of C_1, C_2, and the leakage inductance equal to the switching frequency,

$$C_1 = \frac{1}{\omega_s^2 (L_1 - M)}, \qquad C_2 = \frac{1}{\omega_s^2 (L_2 - M)}, \tag{3}$$

with v_1 and v_2 approximately in phase (**Fig. 6(b)**).

B. Transformer Set-up

The air-core transformer is implemented with two coaxially arranged primary and secondary windings (cf. **Fig. 4**). Both windings are arranged as cylindrical solenoids that are realized with HF litz wire conductors. Single-layer windings are assumed for both primary and secondary coils. The results presented in **Section IV-B** are based on 2–D finite-element method (FEM) simulations and selected results are verified by means of 3–D FEM simulations in **Section IV-D**. The 3–D FEM simulations are conducted without and with magnetic shielding plates that are used to close the flux path and/or limit the magnetic stray field.

C. 2–D FEM-Based Design and Optimization

Different approximations of the transformer configuration depicted in **Fig. 4** can be considered. One approximation is to run separate 2–D FEM simulations for the two sets of coils, I and II, and determine the final values for inductances and couplings from the electric series connection of both sets of coils. Another 2–D approximation considers the placement of coils I and II coaxially in series such that a single set of coils with a length of $2l$ results. The first approach fully decouples coils I and II and underestimates the coupling,

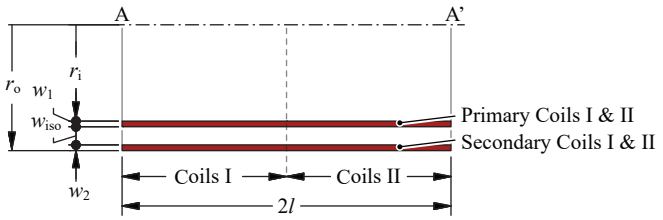

Fig. 7. Schematic representation of the 2–D axisymmetric model (in r–, z–spatial coordinates) of one set of the coils as used for the FEM simulation.

whereas the second approach overestimates the coupling. In this paper, the second approach has been selected with the corresponding axisymmetric 2–D FEM model shown in **Fig. 7**. A detailed investigation of the accuracies achieved with both approaches is subject to further research. The employed 2–D model considers no shielding plates. Furthermore, the primary coil (inner solenoid) is separated from the secondary coil (outer solenoid) by an isolation distance of width w_{iso}.

Fig. 8 depicts the design procedure and optimization of the transformer, which utilizes analytical calculations and FEM simulations. The system specifications listed in **Table I** are providing the input parameters. Second, for the investigated winding arrangements the space of geometry dimensions is defined in **Table II**. For each geometry a FEM simulation is performed with values of self-inductances and mutual inductance normalized to the number of turns, i.e. a single turn inductor. In addition, the values of external magnetic fields and current densities are extracted for the calculation of litz wire losses. Finally, all obtained results are stored in a look-up table, which then is used for analytical calculations. In the next loop, a sweep through switching frequency and number of turns is realized. In this loop the normalized values of parameters obtained from FEM are scaled and the converter compensation method is chosen based on the magnetic coupling value. Using the presented formulas (1)–(3) and an electric model of the SRC (cf. **Fig. 9(a)**), the resonant capacitances, the primary and secondary currents, and losses in the litz wire windings are calculated. The additional copper losses due to skin and proximity effects in each litz wire conductor are calculated based on the peak current and magnetic field values obtained

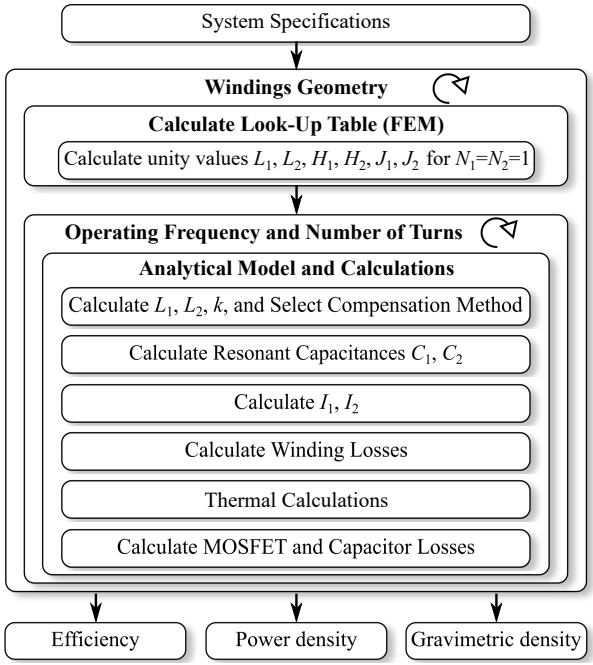

Fig. 8. Flowchart of the implemented optimization procedure for the MV/HF air core transformer.

TABLE II. Design space for the optimization

Var.	Min.	Max.	# Points	Description
2–D FEM Sweep				
f_s	20 kHz	200 kHz	15	switching frequency
N	30	200	170	number of turns
r_i	35 mm	105 mm	15	internal diameter
w_1	5 mm	60 mm	15	width of primary winding
w_2	5 mm	60 mm	15	width of secondary winding
l	60 mm	350 mm	15	length of transformer
3–D FEM Sweep				
s_d	50 mm	80 mm	4	shielding plate distance from end of transf. coils
s_w	4 mm	9 mm	15	thickness of shielding plate
d	1.05	1.20	4	shielding plate to transformer cross section ratio[1]

[1] $s_a = d \cdot 4r_o$, $s_b = d \cdot 2r_o$, cf. **Fig. 4**

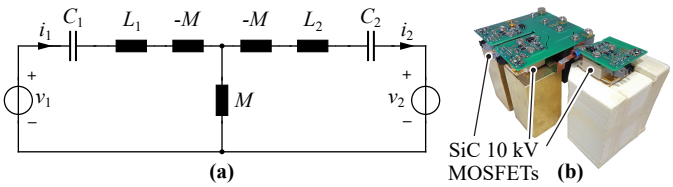

Fig. 9. (a) Lossless electric model of the SRC. (b) 10 kV SiC MOSFET based half-bridge setup for calorimetric measurements of zero voltage switching (ZVS), i.e. soft-switching, losses [16].

from FEM simulation (superposition of scaled vectors of magnetic fields and integration of the loss density according to the models presented in [22]). Furthermore, to ensure thermal feasibility, a thermal model is considered. The transformer designs which exceed a surface related power loss density of $p_{\mathrm{v,max}} = 0.25$ W/cm^2 are removed from the calculated designs. The limit value for thermal calculation is based on [22] where the transformer is assumed to have active cooling, i.e., fans, and both, inner and outer, surfaces are considered as participating in the heat transfer.

D. 3–D FEM-Based Design and Optimiz. w/ Shielding Plates

The 3–D FEM simulations of the air-core transformer are conducted for the actual physical configuration with splitted primary- and secondary-side coils, i.e., two sets of coils, such that the external magnetic fields cancel. The simulations are conducted with and without shielding plates, for closing the flux path and/or for limiting the magnetic stray field (back iron for limiting stray fields), for three selected, optimal 2–D designs. The results are presented and discussed in **Section IV-D**.

Ferrite shielding plates (material N97) with rectangular cross sections are assumed to be two equal cores, placed at both ends of the splitted coils according to **Fig. 4**. For the 3–D models parameter sweeps for different geometries of plates are conducted, similarly to the procedure in **Fig. 8**. However, only one optimization loop is realized since for one design the operating frequency and the number of turns are constant. Therefore, instead of the windings geometry sweep, the distances between coils and the plates, thicknesses, widths, and lengths of the plates are varied (cf. **Table II**). For each configuration, the model is solved and all performance indexes are calculated and stored. The modeled transformer has three planes of symmetry, thus, to reduce the computational effort, mirroring is used in all planes to simplify the model.

III. Conventional MV/MF Transformer

In case of a conventional MV/MF transformer (magnetic core based transformer, MCT), the design of the SRC requires

the values of leakage and magnetizing inductances, which are obtained from the transformer geometry. Furthermore, it involves the calculation of the resonant capacitances, which are calculated in order to obtain a resonance frequency equal to the switching frequency. In the SRC with leakage inductance compensation, the magnetizing inductance provides a basic inductive load to the full bridges on the primary and secondary sides. With this, ZVS, i.e. complete charging and discharging of all MOSFETs' output capacitances, is achieved for the complete power range.

In this study, the MCT is used as a reference and for comparison with the air-core transformer (ACT) for the same application and specifications as presented in **Table I**. The design and optimization of the MCT transformer is well documented in the literature, therefore, in this paper, the MCT is designed and optimized based on the routine and models presented in [23]. The considered MCT consists of E-cores (ferrite N95) and shell-type windings. The winding loss model includes skin and proximity losses in the litz wire conductors [23]. For the calculation of the ferrite core losses the improved Generalized Steinmetz Equation (iGSE) is used [24]. Furthermore, similarly to the ACT, the thermal model is based on the surface related power loss density of the transformer. Finally, the value of magnetizing current required for ZVS is set by introducing an air gap of suitable length.

IV. Evaluation

To complete the analysis, the remaining elements of the converter, such as transistors, resonant and dc-link capacitors, and the cooling system, are evaluated. In the final stage of the optimization, losses, volumes, and masses of those components are calculated. Finally, only the Pareto-optimal designs with respect to efficiency η and gravimetric power density $\gamma\,(\mathrm{kW/kg})$ and volumetric power density $\rho\,(\mathrm{kW/dm^3})$ are stored and used for evaluation and comparison.

A. Considered Components

The conduction losses of the SiC MOSFETs are calculated assuming an on-state resistance of $400\,\mathrm{m\Omega}$ as given for a junction temperature of $100°$ [16]. Furthermore, experimental data from the characterization of the soft-switching losses of the SiC MOSFETs, obtained with the setup presented in **Fig. 9(b)**, are used to calculate the switching losses for $7\,\mathrm{kV}$ dc input and $7\,\mathrm{kV}$ dc output voltage. In addition, the number of parallel dies per switch is limited to 3 and the maximum losses are set to $100\,\mathrm{W}$ per die. For resonant and dc-link capacitors the losses are estimated using the dissipation factors specified in the data sheets, i.e., 0.05% and 0.1% respectively. The capacitor models of volume and mass use the scaled energy density factors of existing designs, i.e., for the resonant capacitors $2\,\mathrm{J/dm^3}$ and $1\,\mathrm{J/kg}$ [22] and for the dc-link capacitors $40\,\mathrm{J/dm^3}$ and $30\,\mathrm{J/kg}$ [16]. Furthermore, the peak voltage of resonant capacitors is limited to $10\,\mathrm{kV}$. Volume, mass, and losses of the cooling system are based on experimental data from [16].

B. η-γ-ρ-Pareto Fronts for ACT and MCT Converters (2–D)

The η-γ-ρ-performance spaces (planes) and the η-γ-ρ-Pareto fronts that result from the 2–D FEM simulations for ACT and MCT transformers with the respective dc–dc converters are shown in **Figs. 10(a)–(d)**. From the η-γ-performance planes shown in **Figs. 10(a)** and **(c)** it becomes apparent that the converter with MCT due to thermal limitation cannot

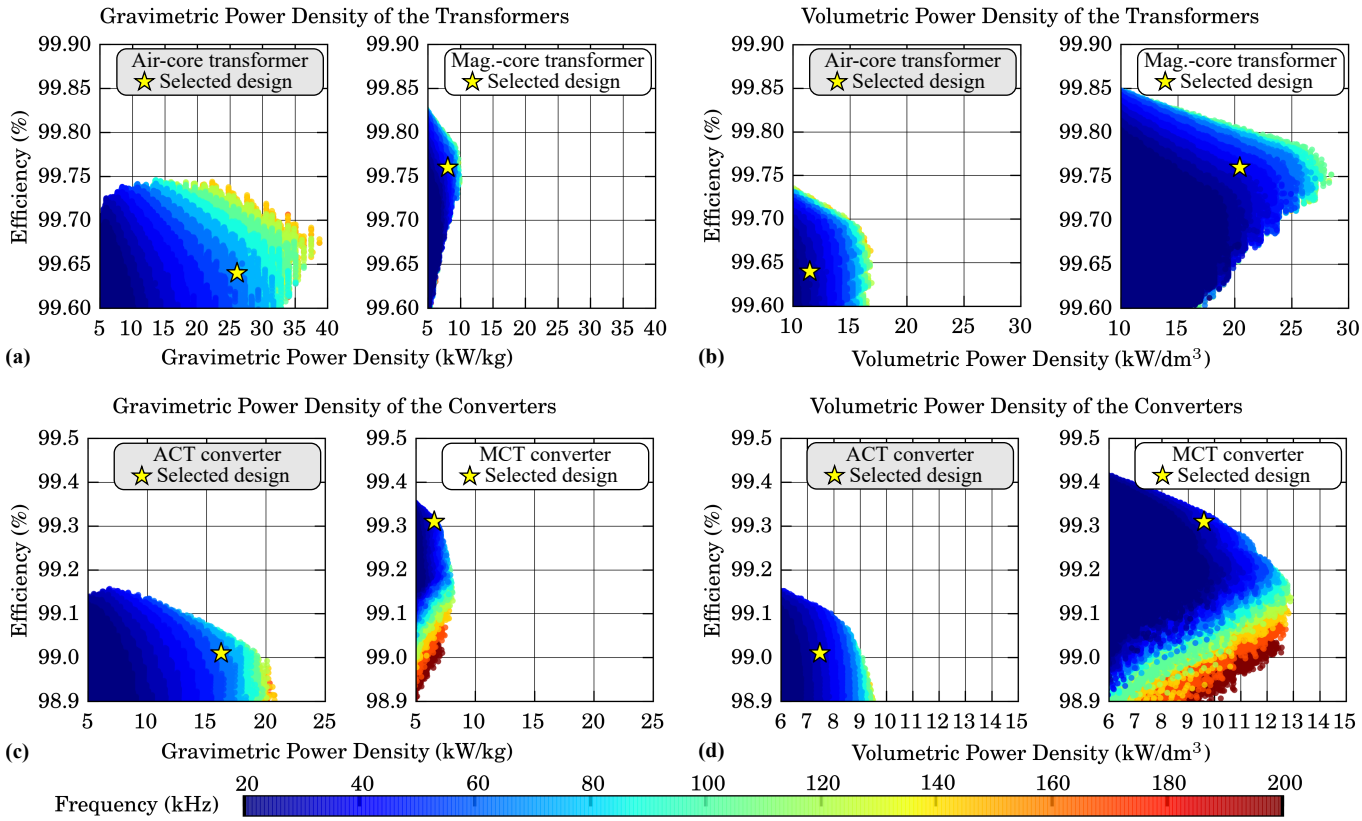

Fig. 10. Results of the 166 kW / 7 kV transformer multi-objective optimization (2–D FEM for the ACT, numerical approx. without FEM for the MCT). η-γ-ρ-performance planes: (a) gravimetric power density γ of the air-core transformer (ACT) vs. the magnetic-core transformer (MCT); (b) volumetric power density ρ of the ACT vs. the MCT; (c) gravimetric power density γ of the overall ACT converter vs. the overall MCT converter (d) volumetric power density ρ of the overall ACT converter vs. the overall MCT converter.

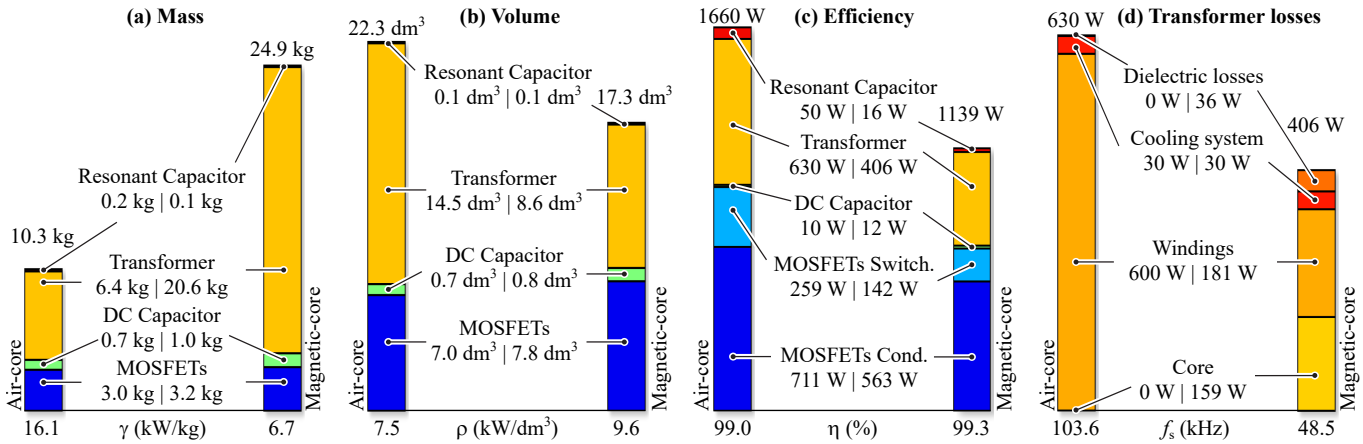

Fig. 11. Break-down of the calculated (a) masses, (b) volumes, (c) losses of the components employed in the two chosen designs. (d) Detailed transformer losses including losses for the cooling system operation.

achieve a power density of more than $8\,\mathrm{kW/kg}$, whereas the converter with ACT can achieve densities higher than $21\,\mathrm{kW/kg}$, while still maintaining a comparably high efficiency of 99.0%. It is worth to point out that, even though there are high-efficient (99.7%) air-core transformer designs (cf. **Fig. 10(a)**) with relatively high switching frequency up to 200 kHz, due to high switching losses of the transistors those designs have poor overall system performance (cf. **Fig. 10(c)**). From the η-ρ-performance plane shown in **Figs. 10(b)** and **(d)** it can be seen that the maximum achievable volumetric power density for an ACT ($17\,\mathrm{kW/dm^3}$) is approximately half of the maximum achievable density of a MCT ($29\,\mathrm{kW/dm^3}$). The larger volume of the ACT can be explained by the fact that either a higher number of turns (long transformer) or a larger diameter of the solenoid windings is needed to obtain effectively the same inductances in comparison to the MCT. According to **Fig. 10(d)**, however, the disproportion of the maximum volumetric power density of the converter is not that significant ($13\,\mathrm{kW/dm^3}$ to $9.5\,\mathrm{kW/dm^3}$) and is in favor of the MCT. For a more detailed comparison one design from each system type is selected for analysis, as indicated by yellow stars in **Fig. 10**. The designs were selected by introducing the following converter performance criteria: efficiency >99.0% and the highest achievable gravimetric power density. For the ACT the selected design is not located on the front of the Pareto plane because such design is not optimal after adding shielding plates, which is explained in more detail in **Section IV-D**. **Figs. 11(a)–(c)** show detailed information about the converter elements' share in overall mass, volume, and losses for the two selected designs, i.e., $\{99.0\%,\ 103.6\,\mathrm{kHz}\}$ for the ACT and $\{99.3\%,\ 48.5\,\mathrm{kHz}\}$ for the MCT. In addition, in **Fig. 11(d)** the breakdown of the losses of the corresponding transformers including cooling systems is presented. It is interesting to notice, that the design with ACT has almost three times higher gravimetric density with a trade-off of only $\approx 0.3\%$ concerning efficiency than a design with MCT, which constitutes a considerable advantage for a weight-critical application.

C. Investigations of Isolation Distances and Insulation in ACT

Further exploration of the design space of the ACT focuses on the inter-winding isolation distance and insulation material. In the analyzed system for the operating voltage of $7\,\mathrm{kV}$ the required withstand voltage for the transformer is chosen to be $10\,\mathrm{kV}$. It can be achieved either with dry-type insulation for small distances or air insulation provided that the distance is at least equal to the air clearance distance for the required withstand voltage and given that no creepage path exists.

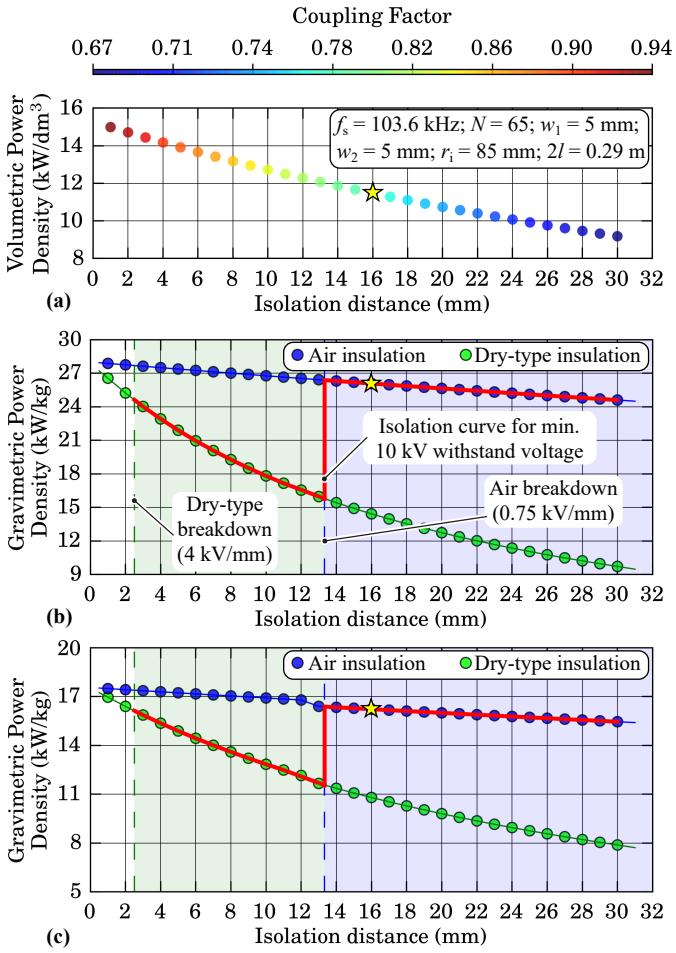

Fig. 12. Volumetric and gravimetric power density for the selected converter with ACT for different isolation distance w_{iso} between the windings and different insulation materials, i.e., air and silicone (from 2–D FEM simulations without shielding plates). (a) Volumetric power density of transformer. (b) and (c) gravimetric power density of transformer and complete converter system, respectively. For the chosen $10\,\mathrm{kV}$ withstand voltage, the breakdown boundaries and the resulting functional isolation curve for the system are plotted.

For the selected ACT design ($\{99.0\%,\ 103.6\,\mathrm{kHz}\}$) additional 2–D FEM simulations were carried out for different isolation distances between the windings $w_{\mathrm{iso}} \in \{1, 2, ..., 30\}$ mm and both insulation types: dry-type (silicone) and air. In case of dry-type insulation, the additional mass of the insulation

material was accounted for in the gravimetric power density. In **Fig. 12(a)** the volumetric power density for ACTs without shielding plates is presented along with the information about the coupling factor which varies from 0.67 to theoretically 0.94 for small isolation distances. **Fig. 12(b)** and **(c)** clearly shows that feasible designs start from the dry-type insulation breakdown boundary (2.25 mm), which is the only possibility up to the air breakdown boundary (13.33 mm). As expected it is more beneficial to use air insulation as significantly higher gravimetric densities can be achieved, since air insulation designs have higher gravimetric power density than dry-type insulation designs with same isolation distance. Furthermore, the selected design ($w_{\text{iso}} = 16$ mm) with air insulation allows to avoid using additional insulation materials and associated challenges such as dielectric losses, and partial discharges [17].

D. η-γ-Pareto Fronts for ACT with Shielding Plates (3–D)

Fig. 13 shows the η-γ-performance space for a converter employing an ACT, achieved from 2–D FEM simulations (without shielding plates, cf. **Fig. 10(c)**). The designs are colored according to the lengths of the transformers. Additionally, three selected designs are shown for reference, for three different transformer lengths $2l \in \{17.5, 22.5, 29.0\}$ cm and efficiencies of 99.0%. Finally, for those three designs the corresponding Pareto optimal results with optimized shielding plates from 3–D FEM simulations are presented considering the shielding plates. The 3–D FEM optimal results are selected with respect to gravimetric power density and from the subset of designs, in which the shielding plates are not in saturation, i.e., the maximum magnetic flux density in plates is below 300 mT.

From **Fig. 13** it can be seen that choosing the optimal design without shielding plates ($2l = 17.5$ cm) does not lead to the best design after adding the shielding plates. In fact, the best performance with shielding plates is achieved for the longest transformer that features the lowest gravimetric density without shielding plates. This relation can be explained by the fact that long transformers are also characterized by smaller outer diameters, which determine the sizes of the shielding plates. More detailed performance indexes of the selected optimal design ($2l = 29$ cm) for all models, i.e., 2–D, 3–D without shielding plates, and 3–D with shielding plates, are shown in **Table III**. Adding the ferrite shielding plates generates additional losses, which causes a reduction of the efficiency of approx. 0.1% and a drop of the gravimetric density from 16.2 kW/kg to 11.5 kW/kg. On the other hand, the shielding plates realize the function of back iron for stray fields, which otherwise could cause eddy current losses in surrounding conductive elements or generate EMI perturbations. In the presented case the shielding plates are reducing the value of the magnetic flux density in axial distance of 94 mm from the end of the coils (1 cm from shielding plates) from 3.0 mT to 0.5 mT (cf. **Fig. 14**), which is below typical values specific for MV magnetic core transformers [17].

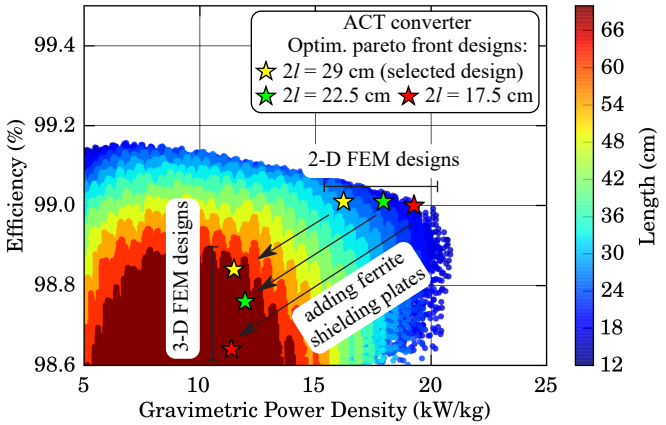

Fig. 13. Results of the multi-objective optimization of the ACT for the ACT converter (166 kW / 7 kV) without shielding plates (2–D FEM simulation) and with shielding plates (3–D FEM simulation) for three designs with different transformer lengths. The mapping of 99% efficient 2–D designs calculated without considering shielding plates (**Fig. 10(c)**) into corresponding optimal 3–D designs with plates is indicated with arrows.

TABLE III. Performance indexes of the selected optimal design ($2l = 29$ mm) of the ACT converter: 2–D, 3–D without shielding plates and 3–D with shielding plates

Solution	Gravimetric density (kW/kg)	Volumetric density (kW/dm^3)	System efficiency (%)	Magnetic flux density - stray field (mT)
2–D	16.2	7.47	99.01	-
3–D without shielding plates	16.2	7.47	98.94	3.0
3–D with shielding plates	11.5	3.97	98.84	0.5

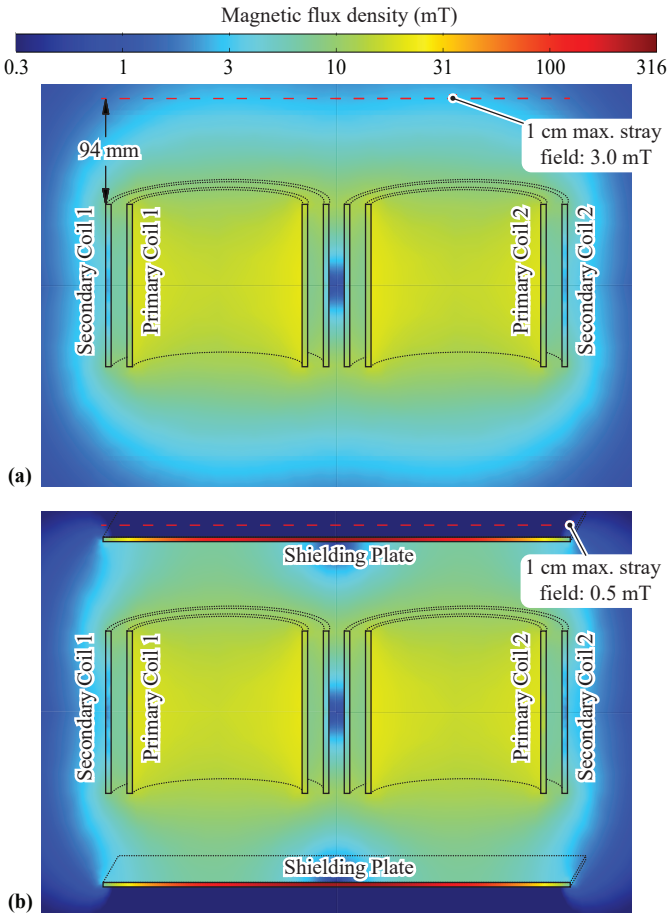

Fig. 14. Results of the 3–D FEM simulation for the selected design: magnetic flux density in the xz–plane. Air-core transformer (a) without shielding plates and (b) with shielding plates. The maximum values of the magnetic flux density in 1 cm proximity from shielding plates are provided.

V. Conclusion

This paper evaluates MV transformers with air-core (ACT) and magnetic-core (MCT) for a 7 kV / 166 kW series-resonant dc–dc converter employed in a multi-cell SST, based on a comprehensive design space exploration. With the use of MV SiC MOSFETs featuring ZVS and a blocking voltage of 10 kV, the converter with ACT can achieve gravimetric power densities higher than 21 kW/kg, while still maintaining comparably high

efficiency of 99.0%, whereas a converter system employing a MCT cannot achieve a gravimetric power density of more than $8\,\mathrm{kW/kg}$, due to thermal limitation of the MCT. The selected Pareto optimal design of the ACT itself is found to enable a lower mass ($10.3\,\mathrm{kg}$ vs. $24.9\,\mathrm{kg}$) and a comparable efficiency of 99.0% at a switching frequency of $103.6\,\mathrm{kHz}$.

One of the challenges in designing MV/MF transformers is the insulation. It is shown that air-core transformers allow to avoid using additional insulation materials and/or the associated challenges (dielectric losses, partial discharges). From the comparison of the air and silicone insulation for the required withstand voltage of $10\,\mathrm{kV}$ for the transformer it is clear that it is more beneficial to use air insulation as higher gravimetric power densities can be achieved.

The ACT employs splitted coils to provide guidance of the magnetic flux along the whole geometric path, and magnetic shielding plates as back iron for limiting the external magnetic stray field. Results from 3–D FEM simulations show that shielding plates are reducing the value of magnetic flux density in an axial distance of $94\,\mathrm{mm}$ measured from the end of the coils from $3.0\,\mathrm{mT}$ to $0.5\,\mathrm{mT}$, which is below typical values specific for MV magnetic core transformers. This solution, however, comes with a significant reduction of gravimetric and volumetric power density, and it is therefore beneficial to use ACTs without shielding plates, if possible.

In summary, the ACT represents an attractive alternative to an MCT for weight-critical applications, e.g., future Turboelectric Distributed Propulsion aircraft. Furthermore, the proposed construction of the ACT is advantageous with regard to insulation coordination and is expected to allow for more effective active cooling compared to MCTs. A scaled hardware prototype with a rated power of $25\,\mathrm{kW}$ is currently under construction in order to verify the presented calculated results, examine the residual external magnetic field, and study the effectiveness of the proposed shielding plates. Besides that, future research will focus on the identification of accuracies of 2–D FEM simulations of advanced configurations when compared to the results of 3–D FEM simulations and/or experimental results, e.g., to enable computationally efficient Pareto-optimizations of configurations with different types of shielding (e.g. plates, bars) and alternative configurations of ACTs. A respective example is the optimization of an arrangement with balanced primary- and secondary-side transformer currents, where primary coil I is placed inside secondary coil I and secondary coil II is placed inside primary coil II.

Acknowledgment

The authors are very much indebted to the Swiss Centre for Competence in Energy Research on the Future Swiss Electrical Infrastructure (SCCER-FURIES) and the National Research Programme on the Energy Turnaround (NRP 70) of the Swiss National Science Foundation (SNSF) for the support of the research in the area of Solid-State Transformer Technology at the ETH Zurich.

References

[1] B. Sarlioglu and C. T. Morris, "More Electric Aircraft: Review, Challenges, and Opportunities for Commercial Transport Aircraft," *IEEE Transactions on Transportation Electrification*, vol. 1, no. 1, pp. 54–64, 2015.

[2] S. Castellan, R. Menis, A. Tessarolo, and G. Sulligoi, "Power Electronics for All-Electric Ships with MVDC Power Distribution System: An Overview," in *Proc. of International Conference on Ecological Vehicles and Renewable Energies (EVER)*, 2014, pp. 1–7.

[3] X. She, A. Q. Huang, and R. Burgos, "Review of Solid-State Transformer Technologies and Their Application in Power Distribution Systems," *IEEE Journal of Emerging and Selected Topics in Power Electronics*, vol. 1, no. 3, pp. 186–198, 2013.

[4] Airbus, "Airbus, Rolls-Royce, and Siemens Team up for Electric Future Partnership Launches E-Fan X Hybrid-Electric Flight Demonstrator." [Online]. Available: http://www.airbus.com/newsroom/press-releases/en/2017/11/airbus–rolls-royce–and-siemens-team-up-for-electric-future-par.html

[5] N. Madavan, "NASA Investments in Electric Propulsion Technologies for Large Commercial Aircraft," in *Proc. of Electric and Hybrid Aerospace Technology Symposium*, 2016.

[6] M. Armstrong, "Superconducting Turboelectric Distributed Aircraft Propulsion," in *Proc. of Cryogenic Engineering Conference / International Cryogenic Materials Conference*, 2015.

[7] M. Callavik, A. Blomberg, J. Häfner, and B. Jacobson, "The Hybrid HVDC Breaker. An Innovation Breakthrough Enabling Reliable HVDC Grids," *ABB Grid Systems, Technical Paper*, 2012.

[8] C. Gu, P. Wheeler, A. Castellazzi, A. J. Watson, and F. Effah, "Semiconductor Devices in Solid-State/Hybrid Circuit Breakers: Current Status and Future Trends," *Energies*, vol. 10, no. 12, p. 495, 2017.

[9] M. Guacci, "Analysis and Design of a 1200 V All-SiC Planar Interconnection Power Module for Next Generation More Electrical Aircraft Power Electronic Building Blocks," *CPSS Transactions on Power Electronics and Applications*, vol. 2, no. 4, pp. 320–330, Dec 2017.

[10] A. T. Isikveren, A. Seitz, P. C. Vratny, C. Pornet, K. O. Plötner, and M. Hornung, "Conceptual Studies of Universally-Electric Systems Architectures Suitable for Transport Aircraft," in *Proc. of 61th Deutscher Luft- und Raumfahrtkongress*, 2012.

[11] J. E. Huber, D. Rothmund, and J. W. Kolar, "Comparative Evaluation of Isolated Front End and Isolated Back End Multi-Cell SSTs," in *Proc. of IEEE International Power Electronics and Motion Control Conference (IPEMC-ECCE Asia)*, 2016, pp. 3536–3545.

[12] N. Soltau, H. Stagge, R. W. D. Doncker, and O. Apeldoorn, "Development and Demonstration of a Medium-Voltage High-Power DC-DC Converter for DC Distribution Systems," in *Proc. of IEEE International Symposium on Power Electronics for Distributed Generation Systems (PEDG)*, 2014, pp. 1–8.

[13] C. Zhao, D. Dujic, A. Mester, J. K. Steinke, M. Weiss, S. Lewdeni-Schmid, T. Chaudhuri, and P. Stefanutti, "Power Electronic Traction Transformer – Medium Voltage Prototype," *IEEE Transactions on Industrial Electronics*, vol. 61, no. 7, pp. 3257–3268, 2014.

[14] M. S. Agamy, M. E. Dame, J. Dai, X. Li, P. M. Cioffi, R. L. Sellick, and R. K. Gupta, "Resonant Converter Building Blocks for High Power, High Voltage Applications," in *Proc. of IEEE Applied Power Electronics Conference and Exposition (APEC)*, 2015, pp. 2116–2121.

[15] D. Han, J. Noppakunkajorn, and B. Sarlioglu, "Efficiency Comparison of SiC and Si-Based Bidirectional DC-DC Converters," in *Proc. of IEEE Transportation Electrification Conference and Expo (ITEC)*, 2013, pp. 1–7.

[16] D. Rothmund, D. Bortis, J. Huber, D. Biadene, and J. W. Kolar, "10kV SiC-based Bidirectional Soft-Switching Single-Phase AC/DC Converter Concept for Medium-Voltage Solid-State Transformers," in *Proc. of IEEE International Symposium on Power Electronics for Distributed Generation Systems (PEDG)*, 2017, pp. 1–8.

[17] T. Guillod, F. Krismer, and J. W. Kolar, "Electrical Shielding of MV/MF Transformers Subjected to High dv/dt PWM Voltages," in *Proc. of IEEE Applied Power Electronics Conference and Exposition (APEC)*, 2017, pp. 2502–2510.

[18] F. Kieferndorf, U. Drofenik, F. Agostini, and F. Canales, "Modular PET, Two-Phase Air-Cooled Converter Cell Design and Performance Evaluation with 1.7kV IGBTs for MV Applications," in *Proc. of IEEE Applied Power Electronics Conference and Exposition (APEC)*, 2016, pp. 472–479.

[19] R. Bosshard, U. Iruretagoyena, and J. W. Kolar, "Comprehensive Evaluation of Rectangular and Double-D Coil Geometry for 50 kW/85 kHz IPT System," *IEEE Journal of Emerging and Selected Topics in Power Electronics*, vol. 4, no. 4, pp. 1406–1415, 2016.

[20] S. Mao, C. Li, T. Song, J. Popovic, and J. A. Ferreira, "High Frequency High Voltage Generation with Air-Core Transformer," in *Proc. of IEEE International Workshop on Integrated Power Packaging (IWIPP)*, 2017, pp. 1–5.

[21] J. W. Kolar, F. Krismer, Y. Lobsiger, J. Mühlethaler, T. Nussbaumer, and J. Miniböck, "Extreme Efficiency Power Electronics," in *Proc. of International Conference on Integrated Power Electronics Systems (CIPS)*, 2012, pp. 1–22.

[22] R. Bosshard, J. W. Kolar, J. Mühlethaler, I. Stevanovi, B. Wunsch, and F. Canales, "Modeling and η-γ-Pareto Optimization of Inductive Power Transfer Coils for Electric Vehicles," *IEEE Journal of Emerging and Selected Topics in Power Electronics*, vol. 3, no. 1, pp. 50–64, 2015.

[23] M. Leibl, G. Ortiz, and J. W. Kolar, "Design and Experimental Analysis of a Medium-Frequency Transformer for Solid-State Transformer Applications," *IEEE Journal of Emerging and Selected Topics in Power Electronics*, vol. 5, no. 1, pp. 110–123, 2017.

[24] K. Venkatachalam, C. R. Sullivan, T. Abdallah, and H. Tacca, "Accurate Prediction of Ferrite Core Loss with Nonsinusoidal Waveforms Using Only Steinmetz Parameters," in *Proc. of IEEE Workshop on Computers in Power Electronics*, 2002, pp. 36–41.